Localized phase jumps in wave trains

J. Lega
Department of Mathematics, Building No. 89, University of Arizona, Tucson, Arizona 85721 and Institut Non Linéaire de Nice, Faculté des Sciences, Université de Nice Sophia-Antipolis, Boîte Postale 71, 06108 Nice CEDEX 2, France

B. Janiaud
Laboratoire de Physique Statistique, Ecole Normale Supérieure, 24 rue Lhomond, 75031 Paris CEDEX 05, France and Research Institute for Electrical Communication, Tohoku University, 2-1-1 Katahira, Sendai 980, Japan

S. Jucquois and V. Croquette
Laboratoire de Physique Statistique, Ecole Normale Supérieure, 24 rue Lhomond, 75031 Paris CEDEX 05, France
(Received 18 September 1991)

We show experimental evidence of traveling hole defects, which are reminiscent of analytical solutions to complex Ginzburg-Landau equations. Also, these objects seem to play an important role in the development of phase instability of oscillatory patterns.

PACS number(s): 47.20.Ky, 47.25.Qv

I. INTRODUCTION

We present an experimental observation of traveling holes in wave trains, reminiscent of those predicted by Bekki and Nozaki [1]. Such objects or defects connect wave trains of different wave numbers, and are characterized by strong localized amplitude and phase variations at their cores. The experiment is Rayleigh-Bénard convection, performed with a fluid of low Prandtl number in an annular cell in which the appearance of concentric rolls is forced above threshold. Under this condition, convective axisymmetric rolls may then become unstable versus an oscillatory instability [2] that leads to the formation of wave trains which propagate along the rolls axis. Under some circumstances, presumably related to the presence of a cell inhomogeneity, a strongly modulated pattern forms, showing a region of lower amplitude, where the wave defects have been observed. This phenomenon is generic since once the depressed area is formed, it travels along the annular cell in a quasistationary manner, presenting phase jumps whose position is apparently uncorrelated with any special location in the cell. Although the stability of the above-mentioned traveling holes has not been studied, they are likely to be unstable [3]. In general, they do not appear spontaneously in ordinary patterns which display stable homogeneous traveling wave trains. We believe that, in our experiment, the strong wave amplitude modulation drives the wave in a highly perturbed state that leads to the formation of traveling holes.

For clarity purposes, we first give a description of the isolated hole solution, together with corresponding numerical simulations. We point out the noticeable features of this traveling-hole [1] defect. Such an idealistic isolated object has not been observed experimentally. Then, we turn to the experimental situation where we believe to evidence several coupled traveling holes in a modulated wave train [4, 5]. They exist for a finite period of time. Finally, we support this observation by comparing the experimental results with a numerical simulation where we initially impose a strong wave modulation that gives rise to transient holes.

II. THE TRAVELING-HOLE SOLUTION

Traveling holes [1] are analytic solutions to the complex Ginzburg-Landau equation. The latter describes the evolution of oscillatory patterns [6], and turns out to be also appropriate for the description of traveling waves.

A. Amplitude equations for a wave pattern

The oscillatory instability of Rayleigh-Bénard convective rolls takes the form of waves that propagate along the rolls axis. These waves are easily visualized by the wiggling shape of the cold stream of the roll pattern. As we have already shown [7], they may be described by means of two coupled Ginzburg-Landau equations:

$$\begin{aligned}\tau_0(\partial_t - V_g\partial_x)A &= \epsilon A + \xi_0^2(1+ic_1)\partial_x^2 A \\ &\quad -g(1+ic_2)(|A|^2+\beta|B|^2)A, \\ \tau_0(\partial_t + V_g\partial_x)B &= \epsilon B + \xi_0^2(1+ic_1)\partial_x^2 B \\ &\quad -g(1+ic_2)(|B|^2+\beta|A|^2)B.\end{aligned} \tag{2.1}$$

In this description, the position of the cold stream is given by

$$y = A\exp[i(-k_0x+\omega_0t)]+B\exp[i(k_0x+\omega_0t)]+\text{c.c.}+\cdots, \tag{2.2}$$

where k_0 and ω_0 are the critical wave vector and frequency measured at threshold, and A and B are the slowly varying amplitudes of the right and left traveling

waves that appear at threshold. The parameters ξ_0 and τ_0 are respectively the correlation length and the characteristic time of the system, and V_g is the group velocity. The temporal frequency above threshold depends on the spatial wave number through c_1, and on the amplitude of oscillations through c_2. If we introduce dimensionless quantities $A' = \sqrt{g/\epsilon}A$, $B' = \sqrt{g/\epsilon}\,B$, $x' = \sqrt{\epsilon}x/\xi_0$, $t' = \epsilon t/\tau_0$, we get the following equations (after dropping the primes):

$$(\partial_t - c\partial_x)A = A + (1+ic_1)\partial_x^2 A - (1+ic_2)(|A|^2 + \beta|B|^2)A, \tag{2.3}$$

$$(\partial_t + c\partial_x)B = B + (1+ic_1)\partial_x^2 B - (1+ic_2)(|B|^2 + \beta|A|^2)B,$$

where $c = V_g\tau_0/(\sqrt{\epsilon}\xi_0)$. Then, we have only three relevant parameters, namely c_1 and c_2 already described above, and β whose real part rules the competition between traveling [($A = 0$ and $B \neq 0$) or ($A \neq 0$ and $B = 0$)] and standing (A and B both finite) waves.

B. Traveling holes

In [1], Bekki and Nozaki give analytic solutions to the complex Ginzburg-Landau equation

$$\partial_t A = A + (1+ic_1)A_{xx} - (1+ic_2)|A|^2 A, \tag{2.4}$$

that they describe as "traveling holes." They can be written in the form

$$A = \frac{b_1\exp(\kappa\xi) + b_2\exp(-\kappa\xi)}{[\exp(\kappa\xi)+\exp(-\kappa\xi)]^{(1+ia_0)}}\exp[i(Kx-\Omega t)], \tag{2.5}$$

where $\xi = x - c_{\rm th}t$. The complex quantities b_1 and b_2, as well as the real constants κ, K, Ω, and a_0, depend on the parameters c_1 and c_2 that appear in the Ginzburg-Landau equation (2.4). A plot of the amplitude and the phase of A corresponding to one of these traveling-hole solutions is shown in Fig. 1. Each solution connects two waves with different wave vectors. Namely, when $\kappa > 0$, the solution behaves like a homogeneous wave of amplitude $|b_1|$ and wave vector k_1 as $\xi \to +\infty$; for $\xi \to -\infty$, it corresponds to a wave of amplitude $|b_2|$ and wave vector k_2. These asymptotic plane waves are solutions to (2.4) and are given by

$$A_{1,2} = \sqrt{1-k_{1,2}^2}\exp[i(k_{1,2}x + \Omega_{1,2}t)] \tag{2.6}$$

where

$$\Omega_{1,2} = -c_2 + (c_2 - c_1)k_{1,2}^2.$$

At $\xi = 0$, the two waves meet, leading to a localized amplitude depression (or hole) as well as a strong phase gradient. The latter is related to the phase shift $\sigma = \arg(b_1, b_2)$ between the two asymptotic waves [8]. It has to be emphasized that the phase of A has no discontinuity at that point (see enlargement of the core region in Fig. 2). The amplitude of A does not reach zero at the core of the solution, but a minimal value that depends on σ. The amplitude depression is maximal when σ equals π. Only for this value, $A = 0$ at $\xi = 0$. Finally, let us stress that traveling holes are not stationary in general,

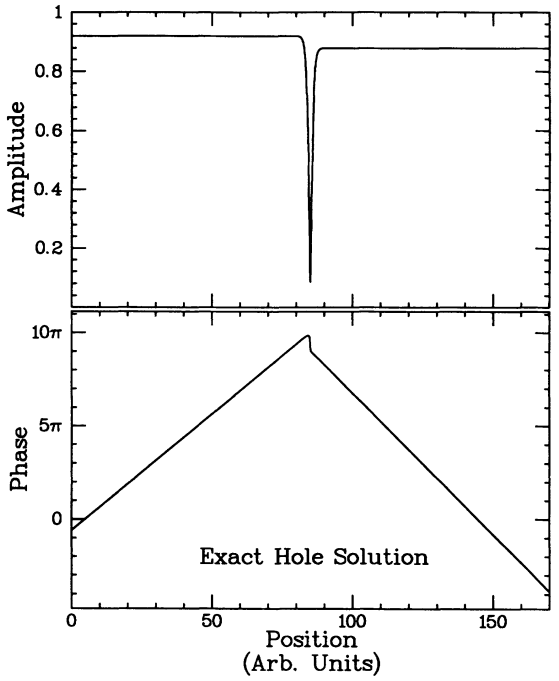

FIG. 1. Plot of the amplitude and the phase of a traveling-hole solution [1] of Eq. (2.4) with $c_1 = 0.5$ and $c_2 = 2.3$. The asymptotic wave numbers are $k_1 = 0.392$ and $k_2 = -0.477(2)$.

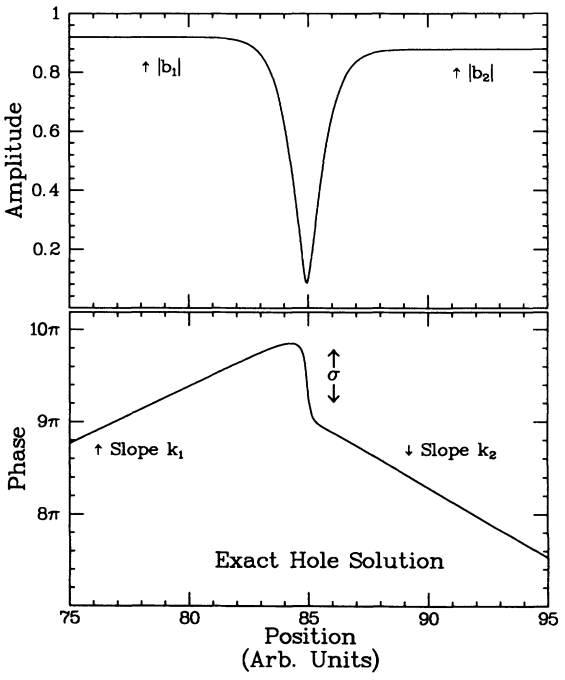

FIG. 2. Enlargement of Fig. 1 about the core of the traveling hole.

but travel at a speed c_{th} [see (2.5)], given by

$$c_{th} = (c_1 - c_2)(k_1 + k_2).$$

This velocity is nothing but the mean value of the group velocities of the two asymptotic waves. It is zero when $\sigma = \pi$.

For given values of the external parameters c_1 and c_2, there exists a one-parameter family of traveling holes [1] that can be parametrized by one (say k_1) of the two asymptotic wave numbers k_1 and k_2. They must satisfy [1] an equation of the form

$$\frac{(k_1 + k_2)^2}{a_1^2} + \frac{(k_1 - k_2)^2}{a_2^2} = 1, \tag{2.7}$$

where a_1 and a_2 depend on c_1 and c_2. Then, an easy way [1] to find the asymptotic wave numbers of a traveling-hole solution consists in finding its velocity c_{th} and reporting its value on the graph of Fig. 3(a), which has been obtained from Eq. (2.7). The two values k_1 and k_2 are then read at the intersection of the ellipse with the straight line $c = c_{th}$. The value of the phase shift σ can be obtained in the same way by means of Fig. 3(b). This graph shows that the possible speeds of traveling holes lie in an interval $-c_{max} < c_{th} < c_{max}$. When $c_{th} = \pm c_{max}$, k_1 and k_2 are equal, and σ goes to 0 or 2π. In this limit case, the two asymptotic plane waves are identical, and the hole disappears. If $k_1 = -k_2$, we recover the stationary hole solution, or "black soliton," described in [9] and [10]. The possible values of k_1 and k_2 are also bounded by $\pm k_{max}$ [see Fig. 3(a)]. The velocities associated with $\pm k_{max}$ are different from c_{max}.

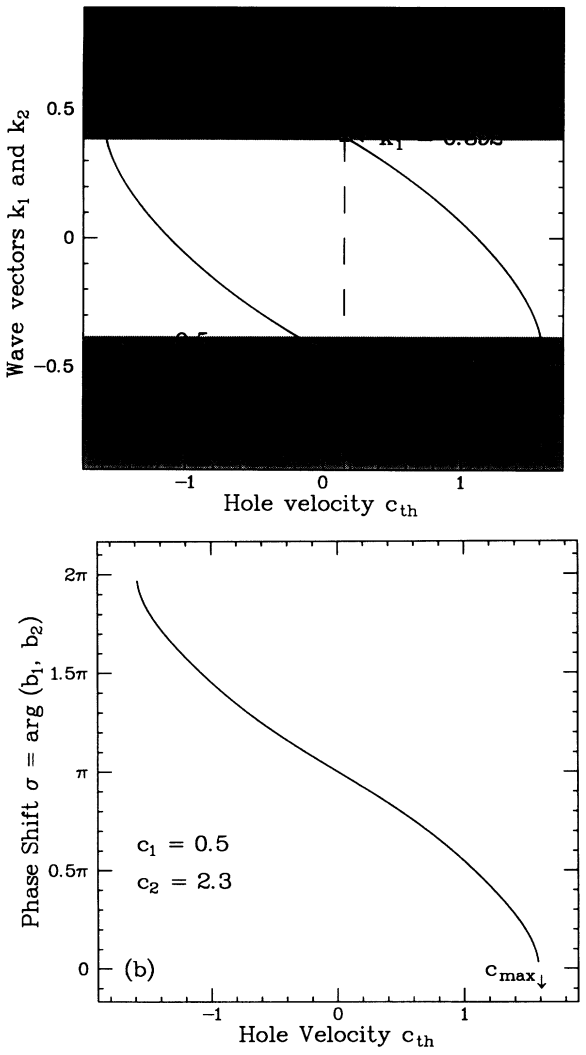

FIG. 3. (a) Asymptotic wave numbers k_1 and k_2 of the hole solutions [1] vs their speed c_{th}. The figure corresponds to $c_1 = 0.5$ and $c_2 = 2.3$. We have shaded the wave numbers that are phase unstable. We have marked the k_1 and k_2 values that correspond to Fig. 1, and shown the associated hole velocity (vertical dashed line). (b) Phase jump σ between the two asymptotic waves vs the hole velocity c_{th}, for $c_1 = 0.5$ and $c_2 = 2.3$.

C. Traveling holes in wave patterns

We can expect that traveling-hole solutions also exist in the case of two coupled Ginzburg-Landau equations like (2.3). However, since $|A|$ decreases at the core of these defects, $|B|$ should grow about this point, and therefore exhibit a pulse-shaped envelope. We have numerically checked that such solutions are possible for Eqs. (2.3). However, depending on the value of Re(β), we can make $|B|$ so small that it can be considered equal

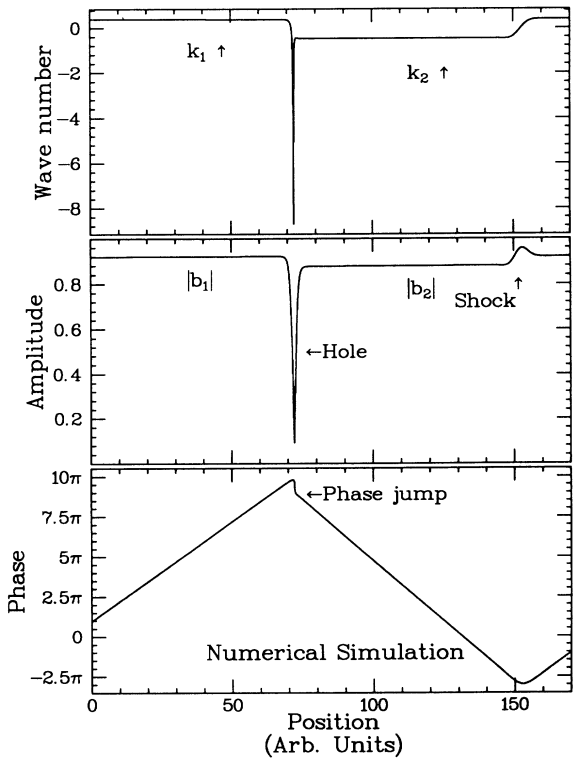

FIG. 4. Numerical simulation of Eqs. (2.3), with $c_1 = 0.5$ and $c_2 = 2.3$. We have plotted the local wave number, the amplitude, and the phase of the complex order parameter A, as functions of space.

to zero everywhere; in this case, its pulse shape disappears. Under these conditions, Eqs. (2.3) can be reduced to a single equation for A, which is nothing but the complex Ginzburg-Landau equation (2.4) written in a frame moving at speed c. Then, traveling-hole solutions to (2.3) are exactly the traveling-hole defects described above. In periodic boundary conditions, a traveling hole is coupled to a shock [1], which connects the two asymptotic states of wave numbers k_1 and k_2, and moves at the same speed c_{th} as the hole. Together, these two objects make a persistent localized pattern [1]. Figure 4 shows a numerical simulation of Eqs. (2.3) with periodic boundary conditions. Here, $\text{Re}(\beta) = 3$ and $|B|$ is always less than 10^{-35}, which is far below the precision of the simulation; in other words, $B = 0$ everywhere. The measured asymptotic wave numbers are $k_1 = 0.392 \pm 0.001$ and $k_2 = -0.477 \pm 0.001$ (same values as in Fig. 1), and the numerically measured instantaneous velocity $c_{\text{num}} = 0.168 \pm 0.01$ falls close to the range given by $c_{\text{th}} = (c_1 - c_2)(k_1 + k_2) = 0.153 \pm 0.004$. The configuration hole shock presented here is not stationary, but the hole slowly changes its asymptotic wave numbers as time goes on. As a consequence, the distance between the hole and the shock slightly decreases in time, while the speed of both increases. This might explain the difference between c_{num} and c_{th}. Nevertheless, these changes are slow enough to allow a good characterization of the traveling-hole solution.

D. Phase stability of the asymptotic waves

Plane-wave solutions to Eq. (2.3),

$$A = \sqrt{1-k^2}\exp[i(kx+\Omega t)], \qquad B = 0, \tag{2.8}$$

are unstable if

$$1 + c_1 c_2 - \frac{2k^2(1+c_2^2)}{1-k^2} < 0,$$

i.e.,

$$1 + c_1 c_2 < 0$$

or

$$k^2 > k_{\text{Eckh}}^2 = 1 \Big/ \left(1 + 2\frac{1+c_2^2}{1+c_1 c_2}\right). \tag{2.9}$$

This criterion [11] corresponds to Benjamin-Feir [12] or Eckhaus [13] instabilities. If $c_1 \to c_2$, Eq. (2.9) gives the usual Eckhaus criterion, where $k_{\text{Eckh}}^2 = \frac{1}{3}$. In this limit situation, only plane waves survive and there are no traveling-hole solutions.

When c_1 and c_2 are different and not equal to zero, the ellipse of Fig. 3 leads to $k_1 \neq k_2$, and $k_{\max}$ may become greater than k_{Eckh}. This means that pairs (k_1,k_2) exist with either k_1 or k_2 falling in the unstable band defined by Eq. (2.9). In Fig. 3, we have shaded the region of unstable wave numbers, for the values of $c_1 = 0.5$ and $c_2 = 2.3$. We find that every hole solution has at least one wave number which is phase unstable and, in some cases, both. This last case corresponds to the pattern of Figs. 1 and 2. However, finite-size effects prevent the development of the instability in this particular case (another possibility could be the existence of an absolute-convective instability threshold, as pointed out in [14] for spiral defects).

III. DESCRIPTION OF THE EXPERIMENT

A. Apparatus

We have studied the evolution of wave trains due to the oscillatory instability in an annulus, using an apparatus similar to the one described in [15]. The control parameter of the experiment is the Rayleigh number Ra which is proportional to the temperature difference ΔT applied to the fluid layer. In this experiment we have used a large-aspect-ratio cell with an outer diameter of 39.7 mm, an inner diameter of 30 mm, and a thickness of 1.18 mm. We had imbedded a resistive wire inside both circular walls made of molded plastic. We adjust the electrical current flowing in these resistances so that the horizontal temperature gradient, produced in this manner, stabilizes a two-concentric-roll pattern in the cell. The radial width of the cell was chosen so that the first instability encountered while increasing Ra is the oscillatory instability. The pattern is visualized using the shadowgraphic method [16]; the cold stream between the two concentric rolls acts as a focusing lens, and produces a white line on the camera image.

B. Data acquisition

The spatiotemporal evolution discussed later takes advantage of the ability of recording the wave evolution at each point in the cell in real time. We now briefly explain how we achieve this measure. When Ra is smaller than the critical value for oscillations Ra_{co}, the roll pattern is stationary and the cold stream separating the two rolls forms a regular circle. Above Ra_{co} the oscillatory instability leads to the development of wavy undulations of this circle. Using a frame grabber in a personal computer, we record the space-time evolution of this white line. We have chosen a square pixel camera synchronized with the horizontal clock of the frame grabber so that the white line appears as a perfect circle. Inside the 512 x 512 pixel image, we define 256 radial segments equally spaced on the circle and extending over 16 pixels. These 256 x 16 pixels correspond to the data that we actually record for each time step. Storing this information on a disk every three TV images, we sample the time dynamics with a frequency of 8.33 Hz, large enough to study the typical 1 Hz frequency of the oscillatory instability. We have been able to record this information over 2048 time steps. After this raw information has been saved, we treat the data: first, for each 16-pixel segment, we estimate the position of the white circle, producing a two-dimensional array of 256 positions for 2048 time steps. Then we achieve some filtering, only in time, for each segment position. By Fourier transform, we apply a bandpass filter to the time information in order to keep only the frequency corresponding to the fundamental frequency of oscillations. Furthermore we reconstruct

a complex signal by keeping only the positive wave number components of the Fourier space and transforming back to the real space. Having a complex signal is very convenient to determine the amplitude of the oscillations and the local wave number, which we measure through the phase shift between the values of the complex signal at two adjacent points.

IV. EXPERIMENTAL RESULTS

A. Time evolution at high Rayleigh number

Above $Ra = 1.2Ra_{co}$, the oscillatory instability always leads to a monotonic evolution with either a clockwise or anticlockwise wave train. After a transient, during which wave trains propagating in opposite directions compete and form sink and source defects, a homogeneous wave invades the entire cell and leads to a monoperiodic spectrum. Different wave numbers have been observed with a mean value corresponding to 38 wavelengths along the annulus. In these states, the amplitude of the wave is fairly homogeneous along the cell, as well as its local wave number. These states remain stable in a wide range of Rayleigh number, provided $Ra > 1.2Ra_{co}$.

B. Time evolution at low Rayleigh number

At low Rayleigh number, homogeneous wave trains become unstable and strong slowly varying amplitude as well as wave-number modulations develop along the pattern. We presume that the origin of the building up of these local modulations is related to a cell inhomogeneity. However, once they have been produced, these modulations do not reflect the cell inhomogeneity since they are not fixed at some spot in the cell but actually slowly turn around the cell. Around $Ra = 1.1Ra_{co}$, these modulations take a simple form: a unique and slowly varying depression of the amplitude of oscillations, and a wave-number modulation in the region of high amplitude. Inside this depression which typically extends over 10 wavelengths, the amplitude is reduced at least by an order of magnitude and the local wave number varies strongly. In the region of large amplitude, the wave number changes nearly by a factor of two between both ends.

Lowering even further the Rayleigh number leads to the formation of several extended amplitude depressions, which are simultaneously present in the cell and separated by wave trains that propagate in opposite directions. Very close to the threshold of the oscillatory instability, the pattern appears as an assembly of small wave trains propagating in both directions and continuously varying in amplitude. Time spectra measured in this state are chaotic. The growth of the amplitude of oscillations seems continuous with Ra and there is no clear region in the cell where the wave trains are smaller in amplitude. However, the chaotic evolution of the wave trains complicates the exact determination of the oscillation threshold.

C. The traveling amplitude depression

We have studied the simplest nonstationary pattern having one amplitude depression turning around the cell. In Fig. 5, we show the shape of the cold stream boundary when this depression is present in the pattern. In Fig. 6, we show the time evolution of the wave train in the entire cell. The grey scale corresponds to the local displacement of the cold stream from its reference circle obtained when no oscillation appears along the rolls. We have recorded

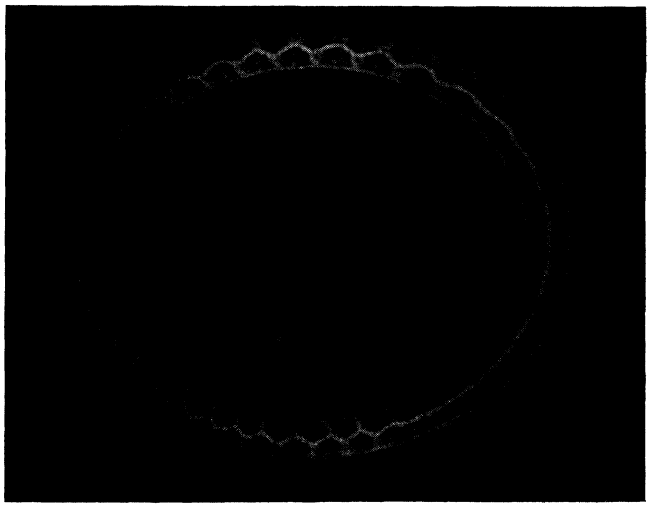

FIG. 5. Shadowgraphic picture of the wave pattern at $\epsilon = 0.1$, for which a single amplitude depression is present. The white line in the annular cell represents the cold stream separating the two concentric rolls. The traveling wave corresponds to the wiggling part of this white line, and is turning clockwise.

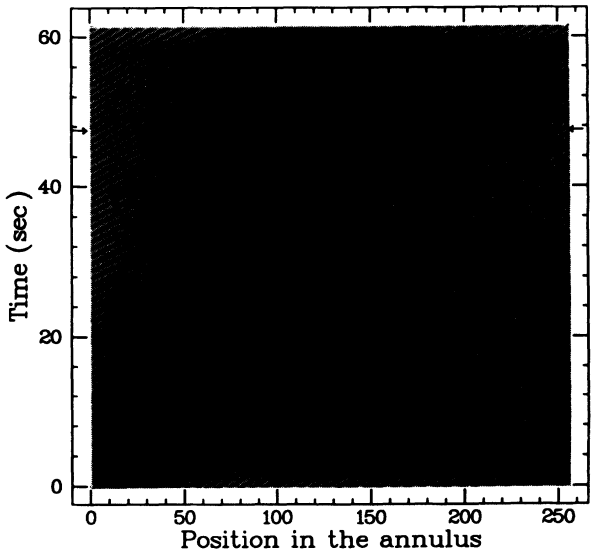

FIG. 6. Space-time evolution of the wave train shown in grey scale. Black (white) pixels correspond to an inward (outward) displacement of the white line with respect to the reference circle. The large amplitude wave depression corresponds to the grey oblique strip in this recording.

this signal over a time long enough so that the amplitude depression (that appears as the grey, slightly blurred region) actually makes more than one turn around the cell. Figure 6 shows only a part of the recorded signal.

The large amplitude wave train presents two very different regions : in a frame moving with the wave train, the leading edge is quasistationary in shape whereas the trailing edge is irregular in time and space. To obtain information on the wave, we have averaged the pattern features (wave number, amplitude) in a moving frame having the same velocity as the amplitude depression. The results are shown in Fig. 7. In the leading edge of the wave train, averaging leads to a noise free pattern having a well-defined amplitude and wave number. In the trailing edge, which typically extends over one quarter of the cell, we observe a noisier structure, corresponding to a region where the pattern is time dependent. In the stationary part of the pattern, the local amplitude and wave number present two plateaus [see Fig. 7(b)], corresponding to a pattern evolution from wave number k_{hi} to wavenumber k_{lo}. This evolution is slow and the wave amplitude adiabatically adapts to the local wave number. Since k_{hi} and k_{lo} are quite different, it is possible to obtain valuable information about the wave-number dependence on the amplitude. By plotting the square of the local amplitude versus the wave number [see Fig. 7(c)], we obtain the expected parabolic shape, whose curvature gives a value of $\xi_0 = 0.42$ compatible with the value of $\xi_0 = 0.57$ obtained in a previous experiment [7].

The trailing edge of the wave train appears to be unstationary. Here, the main feature is the pseudoperiodic nucleation of spatiotemporal dislocations. As may be seen in Fig. 8, the formation of new wavelengths occurs roughly at the same place in the pattern (in a frame moving with the amplitude depression); on the other hand, the disappearance of wavelengths follows a more random mechanism. The interesting phenomenon that we want to emphasize here is that each dislocation nucleation produces a phase jump (seen as a white or dark line) which propagates in the pattern and in most cases leads to the occurrence of a dislocation of opposite sign. Although it is not surprising to see a dislocation producing a phase jump, usually such a phase gradient diffuses, but does not propagate. In Fig. 8, where we have displayed the

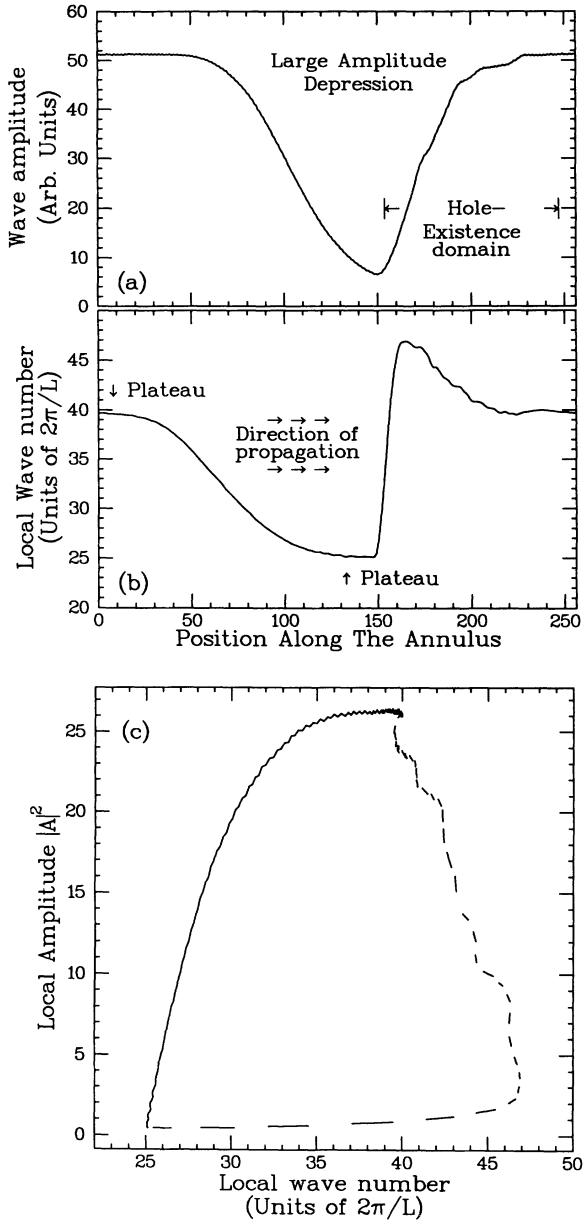

FIG. 7. This series of figures represents the wave features obtained by averaging in the frame moving with the amplitude depression. (a) Wave amplitude. Note the strength of the depression. (b) Local wave number. Note that, in the leading edge of the wave train, the wave number evolves smoothly from 39 to 25. (c) Square of the amplitude vs local wave number, obtained from the data corresponding to the leading edge.

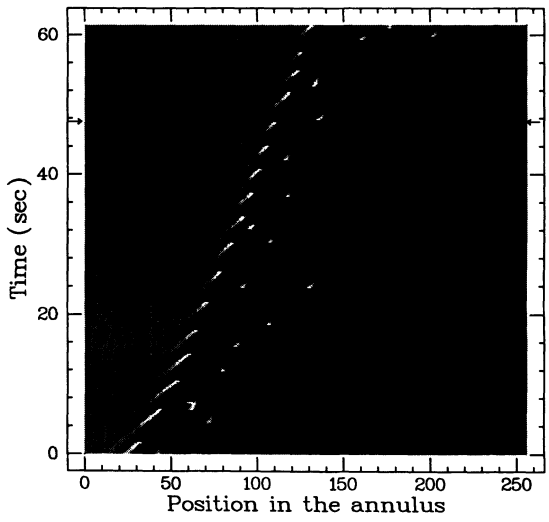

FIG. 8. Space-time evolution of the local wave number. The grey scale corresponds to 80 for black lines and 0 for white ones. These limits extend far beyond the range of linearly unstable wave numbers (25–50). Thus the black ($k = 80$) and white ($k = 0$) lines visible here correspond to phase jumps in the pattern.

local wave number in grey scale, phase jumps correspond to high values of the local wave number and thus appear as white or dark lines. We emphasize that the wave numbers corresponding to either white or black lines are not linearly unstable [17] according to the results of Fig. 7(c), which means that these wave numbers cannot correspond to a propagating wave, but are the signature of a phase jump. All the white and black lines clearly propagate with a relatively similar velocity, which differs from the velocity of the wave train. At the location of each phase jump, the wave amplitude drops to a small value over a short distance (typically one or two wavelengths); we shall refer to this structure as a "hole." In Fig. 9, we present the wave shape along the cell, where both the extended amplitude depression and holes of amplitude may be seen. The velocity of the holes is typically twice as big as that of the amplitude depression.

Finally, bursts of wave trains propagating in the direction opposite to that of the large wave train often appear, starting from the large amplitude depression; however, they never reach an amplitude larger than one tenth of the dominant wave component, and always disappear. Apparently, this wave component has no significant effect on the evolution of defects. This is not the case at lower Rayleigh number, since waves propagating in both directions have similar amplitudes.

To summarize, we observe the spontaneous creation of traveling dips in a traveling wave pattern. They appear in a region of low amplitude and propagate through it. They change their depth and the value of the phase jump at their core as they move. In the following, we give a possible mechanism for this phenomenon. More precisely, we show that traveling holes reminiscent of the analytic solutions described in Sec. II may spontaneously be created in an amplitude depression of a wave pattern.

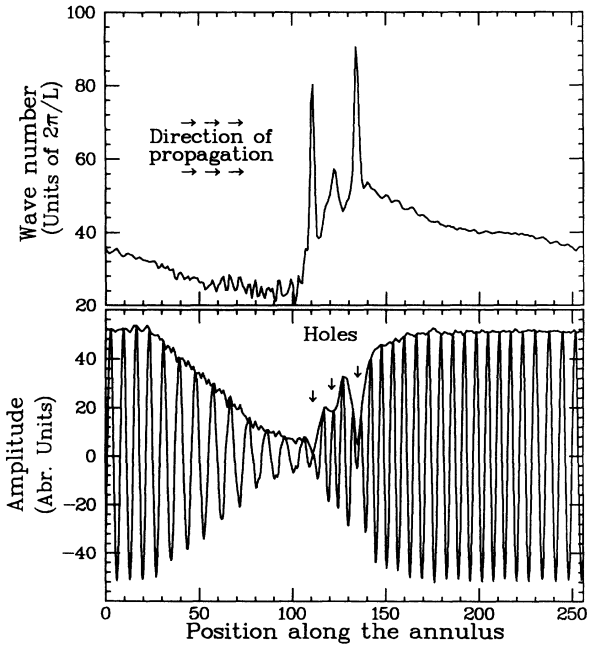

FIG. 9. Wave profiles sampled at a given time (indicated by the arrows on Figs. 6 and 8). Top: local wave number of the wave profile shown in the bottom graph; notice the three peaks indicating the holes. Bottom: displacement of the cold stream and its amplitude versus space. The amplitude depression extends over ten wavelengths, whereas the *holes* typically extend over one wavelength.

V. COMPARISON WITH THE TRAVELING HOLES DESCRIBED BY BEKKI AND NOZAKI

A. Phase instability

As shown in Sec. II, traveling-hole solutions also exist for Eqs. (2.3). However, apart from the fact that they travel at constant velocities, they feature no particular dynamics. In order to make a closer comparison with the behaviors observed in the experiment, we need a mechanism to make such objects appear and disappear in time.

To explain the experiment, we want to show that a phase unstable pattern may lead to the formation of holes.

B. Numerical simulation

According to (2.9), we can make unstable a plane wave of wave number k by choosing either $1+c_1c_2$ negative or positive but small, or $1+c_2^2$ (or equivalently $|c_2|$) large. Here, we know from the experiment that we are far from the Benjamin-Feir instability, i.e., $1+c_1c_2$ is neither negative nor close to zero. Thus, we are interested in the dynamics of Eqs. (2.3) when c_2 is large (with $1+c_1c_2>0$) and when initial conditions are such that phase instability will develop. For given values of c_1 and c_2, there is a critical amplitude $|A|_c$ below which plane waves of wave number k and amplitude $|A|=\sqrt{1-k^2}$ are unstable [it is given by $|A|_c=\sqrt{1-k_{\mathrm{Eckh}}^2}$; see formula (2.9)]. We have chosen an initial condition that exhibits a large amplitude depression and a varying wave number, according to the formula $k(x)=\sqrt{1-|A(x)|^2}$. Besides, the amplitude $|A|$ was smaller than $|A|_c$ at the center of the large depression. This reproduces the experimental situation for which we have an amplitude depression and a wave pattern whose amplitude adiabatically adapts to its phase [at least in the trailing edge of the wave train; cf. Fig. 7(c)].

The dynamics of Eqs. (2.3) with such an initial condition is shown in Fig.10. The main feature is that, similarly to what is observed experimentally, objects strongly reminiscent of the above-described analytic traveling-hole solutions appear inside the amplitude depression. However, since such a large amplitude variation is not stable, it disappears soon, but traveling holes keep on appearing and disappearing at random. Each of them is associated with a high phase gradient at its core and travels at a speed different from the group velocity c. The value of this speed is hardly measurable, since the value of the amplitude at the core of a dip, and therefore the

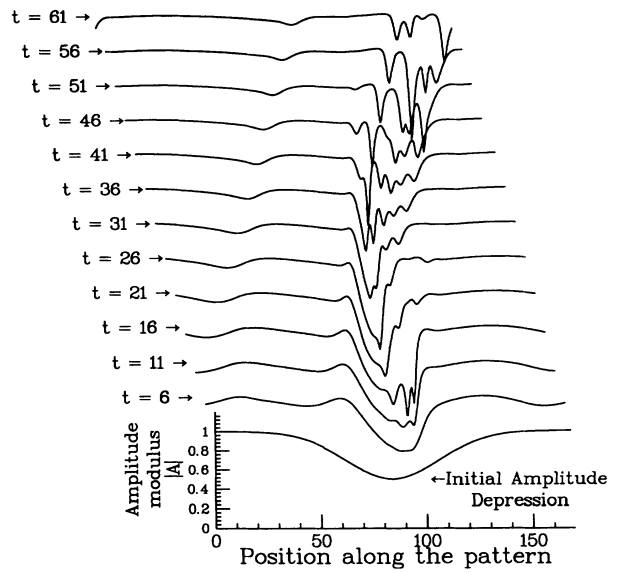

FIG. 10. Numerical simulation of Eqs. (2.3), with $c_1 = 0.5$ and $c_2 = 2.3$. We have plotted the successive amplitude profiles of A, at times t =0, 6, 11, 16, 21, 26, 31, 36, 41, 46, 51, 56, and 61 (in arbitrary units).

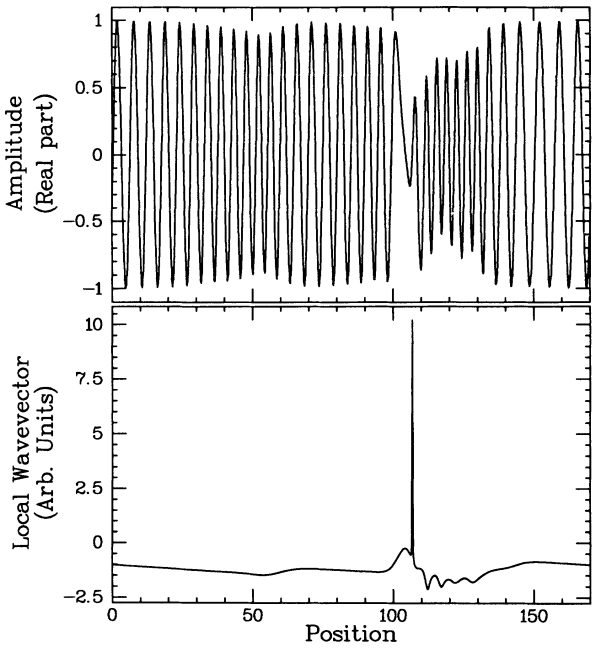

FIG. 12. Wave profile and local wave number at $t = 22$, for the simulation of Fig.10. Note the low amplitude and the high phase gradient at the core of the dip.

dip itself, change in time. Nevertheless, these objects are strongly reminiscent of the analytic traveling-hole solutions described by Bekki and Nozaki. On both sides of the localized region where these dips are observed, the amplitude is space dependent and, as a consequence, the local wave number also varies spatially. Hence, we have the following picture: because of phase instability, amplitude modulations are enhanced, and give rise to the formation of dips that further disappear, while new ones are created. Each time one of them reaches a zero amplitude value at its minimum, A vanishes at this point and this event appears as a spatiotemporal dislocation in the (x,t) diagram for y [given by (2.2)]. However, all dips do not give rise to such dislocations, since most of them first decrease their minimum amplitude and then increase it before it has reached zero. Figure 11 shows the spatiotemporal diagram for the "reconstructed pattern" y associated with Fig. 10, where few dislocations are visible. This is to be compared with Fig. 6. In both figures, note the change of slope of the lines corresponding to the displacement of wavecrests, on both sides of the grey strip. It is due to the slow change of wave number in the region of high amplitude. Till the initial large amplitude depression persists, B exhibits a maximum where A is minimum, and patterns involving two waves are observed in this region. However, $|B|$ is always less than a few percentages of the asymptotic amplitude of A. When the large amplitude depression on A disappears, B can be considered equal to zero everywhere, even at the cores of the traveling holes. The shape of y and the local wave number at time $t = 22$ are shown in Fig. 12, and are to be compared with the experimental pictures of Fig. 9. Eventually, since the homogeneous state is stable, the system restabilizes one traveling hole coupled with a shock.

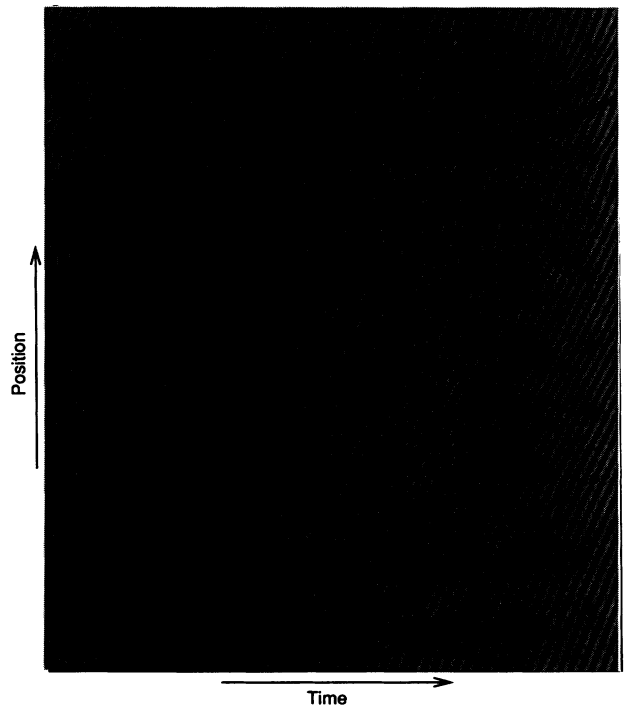

FIG. 11. Spatiotemporal diagram (from $t = 5$ to $t = 31$) for y given by (2.2). It corresponds to the same simulation as in Fig. 10. For the "reconstruction" of y we have chosen $k_0 = \pi 56/170$ and $\omega_0 = 10\pi$.

C. Discussion

We believe that the propagating phase jumps we have experimentally observed in the trailing edge of the wave

train are related to the traveling holes discussed above. More precisely, we know from the numerics that traveling dips which have the same characteristics as the analytic solutions described in [1] can appear spontaneously in an amplitude depression, because of the phase instability of the local wave pattern. The dynamics that ensues is quite similar to what is observed experimentally. We thus have the following interpretation of the experiment. An inhomogeneity of the cell produces a large amplitude depression of the wave pattern. In the leading edge, it corresponds to a change in the wave number, and the latter goes above the Eckhaus instability threshold. The existence of locally unstable wave numbers leads to the formation of traveling holes which propagate through the amplitude depression, and then disappear while new ones are created. The large amplitude depression, which is permanent in the experiment, is not described by the coupled Ginzburg-Landau equations we have considered. That is why the amplitude depression of the initial condition could not persist in the numerical simulation. The existence of a large depression in the experiment has received no convincing explanation yet, though it might be due to large scale flows [18]. We have tried to measure the values of the phase jumps in the experiment, but we always observe several traveling holes simultaneously, which make any accurate measurement difficult. In the same way, the velocity of these defects is relatively well defined, but we do not know the group velocity nor the values of c_1 and c_2 accurately enough to make any reliable comparison.

VI. CONCLUSION

The conclusion of this paper is twofold. First, we have given a detailed description of a rather puzzling pattern observed experimentally, namely a wave train whose local wave number varies in space, and whose leading and trailing edges end in an amplitude depression. We have shown that this is made possible through the creation of traveling holes in this dynamically active region. As shown in the numerical part, their origin is likely to be due to a local destabilization of the pattern. More precisely, they can be spontaneously created in an amplitude depression if the local wave number goes above the Benjamin-Feir-Eckhaus threshold. Second, we have characterized these dips, which are strongly reminiscent of analytic traveling-hole solutions to the complex Ginzburg-Landau equation. From a theoretical point of view, in the same way as point defects are spontaneously created when a two-dimensional pattern becomes phase unstable [19, 20], the appearance of traveling holes seems to be a rule in the time evolution of phase unstable solutions to one-dimensional Ginzburg-Landau equations [21, 22]. It was then of real importance to observe these objects experimentally, since they appear as the one-dimensional analogs of dislocations or spirals, though they are likely to be unstable defects.

ACKNOWLEDGMENTS

We are grateful to D. Bensimon, Y. Couder, P. Coullet, S. Fauve, V. Hakim, A. Newell, T. Passot, A. Pumir, M. Rabaud, P. Tabeling, M.Tabor, and H. Willaime for fruitful discusions. One of us (J.L.) wishes to acknowledge the Arizona Center for Mathematical Sciences (ACMS) for support. ACMS is sponsored by AFOSR Contract No. FQ8671-9000589 (AFOSR-90-0021) with the University Research Initiative Program at the University of Arizona.

[1] N. Bekki and K. Nozaki, Phys. Lett. **110A**, 133 (1985).
[2] R.M. Clever and F.H. Busse, J. Fluid Mech. **65**, 625 (1974).
[3] For a numerical analysis of the stability of the stationary hole, see H. Sakaguchi, Prog. Theor. Phys. **85**, 417 (1991).
[4] Stationary holes seem to have been experimentally observed in a chain of coupled wakes; see P. Le Gal, C. R. Acad. Sci. (Paris) Serie II **313**, 1499 (1991).
[5] Traveling holes may have also been observed in a Taylor-Dean system, as reported in I. Mutabazi, J. Hegseth, C. D. Andereck, and J. E. Wesfreid, Phys. Rev. Lett. **64**, 1729 (1990).
[6] Y. Kuramoto, in *Chemical Oscillations, Waves and Turbulence*, edited by H. Haken, Springer Series in Synergetics Vol. 19 (Springer-Verlag, Berlin, 1984).
[7] V. Croquette and H. Williams, Phys. Rev. A **39**, 2765 (1989); Physica D **37**, 300 (1989).
[8] Formula (5) of Ref. [1] should read $\sigma \equiv \arg(b_2/b_1) = \arctan\left(\{2(p_i/q_i)[(p_r q_i - p_i q_r) + (p_r q_r + p_i q_i)/\alpha]\,\kappa_+\kappa_-\}/[(p_i/q_i)^2|q|^2\kappa_+^2 - (1+\alpha^{-2})|p|^2\kappa_-^2]\right)$.
[9] K. Nozaki and N. Bekki, J. Phys. Soc. Jpn. **53**, 1581 (1984).
[10] F. Cariello and M. Tabor, Physica D **39**, 77 (1989).
[11] J. T. Stuart and R. C. DiPrima, Proc. R. Soc. London, Ser. A **362**, 27 (1978).
[12] A. C. Newell, in *Nonlinear Wave Motion*, Lectures in Applied Mathematics Vol. 15 (American Mathematical Society, Providence, 1974), p. 157.
[13] W. Eckhaus, *Studies in Nonlinear Stability Theory* (Springer-Verlag, New York, 1965).
[14] I. S. Aranson, L. Aranson, L. Kramer, and A. Weber (unpublished).
[15] B. Janiaud, A. Pumir, D. Bensimon, V. Croquette, H. Richter, and L. Kramer, Physica D (to be published).
[16] W. Mesrzkirch, *Flow Visualization* (Academic, New York, 1974); S. Rasenat, G. Hartung, B.L. Winkler, and I. Rehberg, Phys. Fluids. **15**, 379 (1989).
[17] We call linearly unstable wave numbers those that naturally grow above the oscillatory instability threshold. In other words, linearly unstable wave numbers fall inside the parabola of Fig. 7(c).
[18] A. Newell (private communication).
[19] P. Coullet, L. Gil, and J. Lega, Phys. Rev. Lett. **62**, 1619 (1989); Physica D **37**, 91 (1989).
[20] P. Coullet and J. Lega, Europhys. Lett. **7**, 511 (1988).
[21] L. Gil, Nonlinearity **4**, 1213 (1991).
[22] F. Daviaud, J. Lega, P. Bergé, P. Coullet, and M. Dubois, Physica D (to be published).

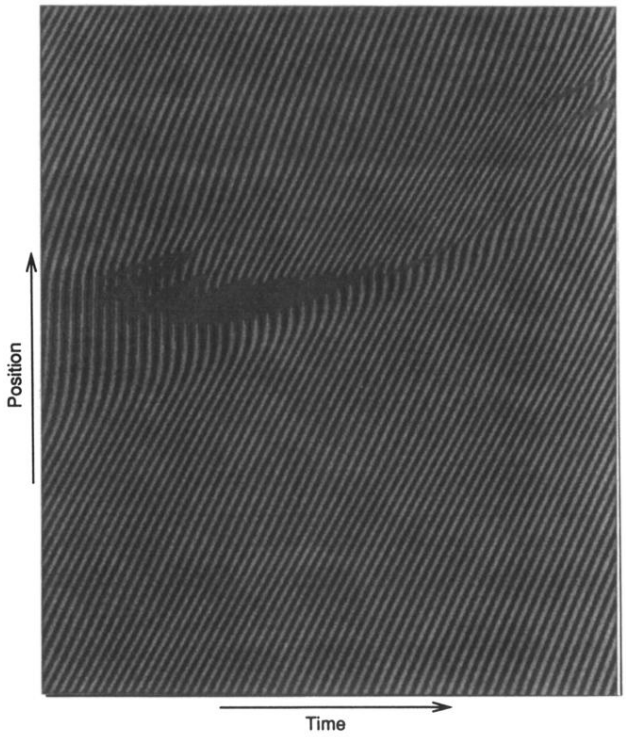

FIG. 11. Spatiotemporal diagram (from $t = 5$ to $t = 31$) for y given by (2.2). It corresponds to the same simulation as in Fig. 10. For the "reconstruction" of y we have chosen $k_0 = \pi 56/170$ and $\omega_0 = 10\pi$.

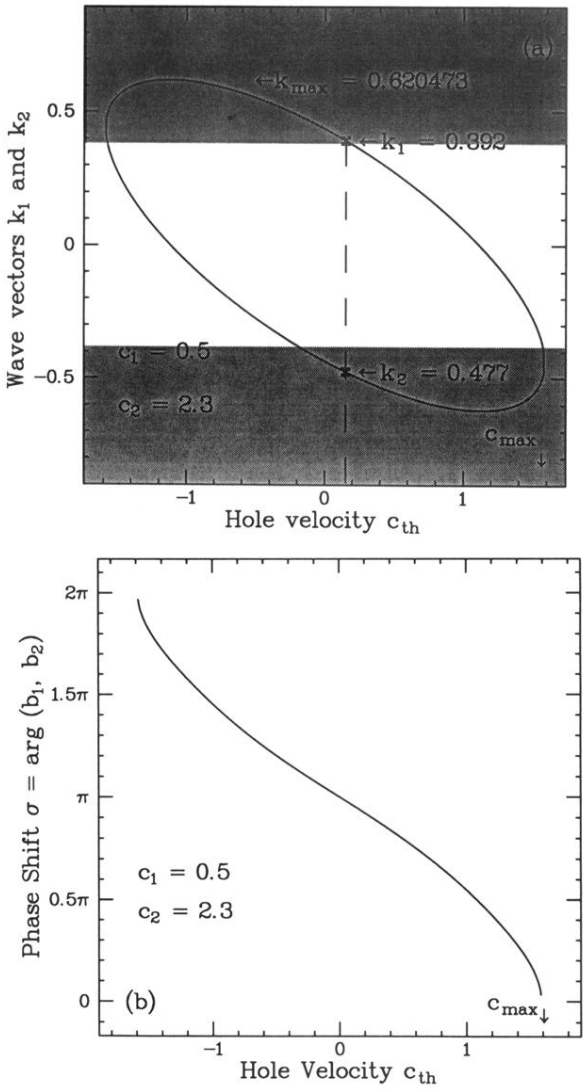

FIG. 3. (a) Asymptotic wave numbers k_1 and k_2 of the hole solutions [1] vs their speed c_{th}. The figure corresponds to $c_1 = 0.5$ and $c_2 = 2.3$. We have shaded the wave numbers that are phase unstable. We have marked the k_1 and k_2 values that correspond to Fig. 1, and shown the associated hole velocity (vertical dashed line). (b) Phase jump σ between the two asymptotic waves vs the hole velocity c_{th}, for $c_1 = 0.5$ and $c_2 = 2.3$.

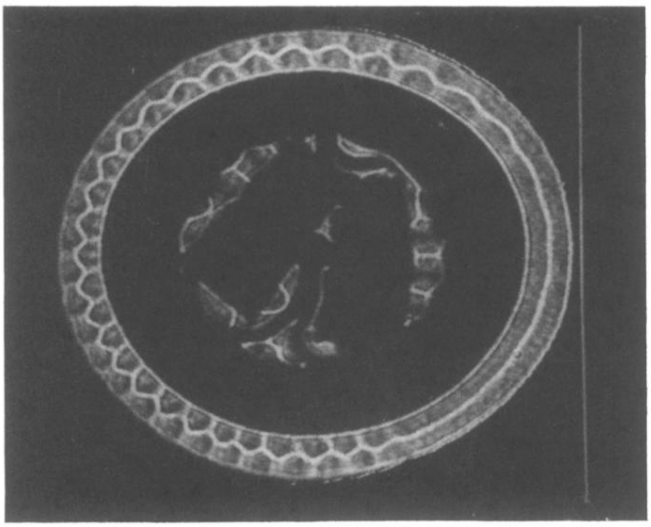

FIG. 5. Shadowgraphic picture of the wave pattern at $\epsilon = 0.1$, for which a single amplitude depression is present. The white line in the annular cell represents the cold stream separating the two concentric rolls. The traveling wave corresponds to the wiggling part of this white line, and is turning clockwise.

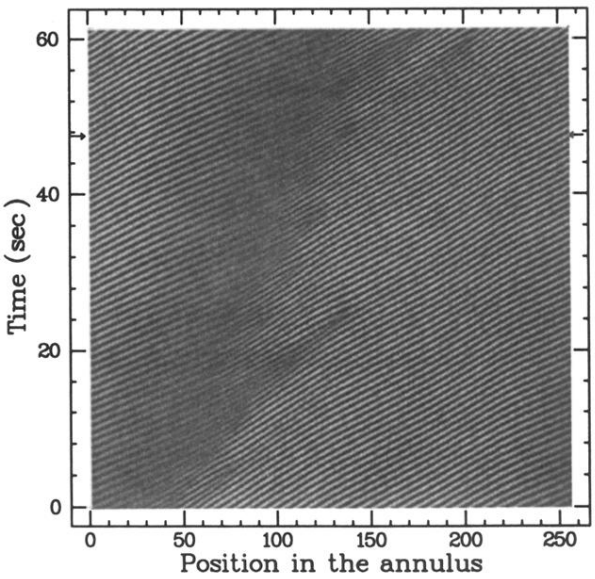

FIG. 6. Space-time evolution of the wave train shown in grey scale. Black (white) pixels correspond to an inward (outward) displacement of the white line with respect to the reference circle. The large amplitude wave depression corresponds to the grey oblique strip in this recording.

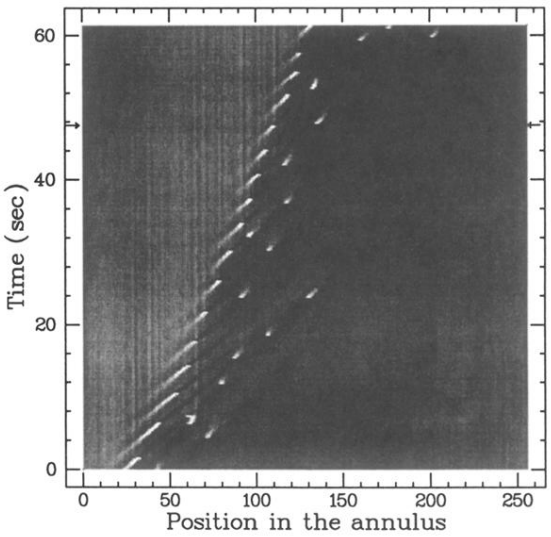

FIG. 8. Space-time evolution of the local wave number. The grey scale corresponds to 80 for black lines and 0 for white ones. These limits extend far beyond the range of linearly unstable wave numbers (25–50). Thus the black ($k = 80$) and white ($k = 0$) lines visible here correspond to phase jumps in the pattern.